Report

Cell Reports

# Gliomas Interact with Non-glioma Brain Cells via Extracellular Vesicles

## Graphical Abstract

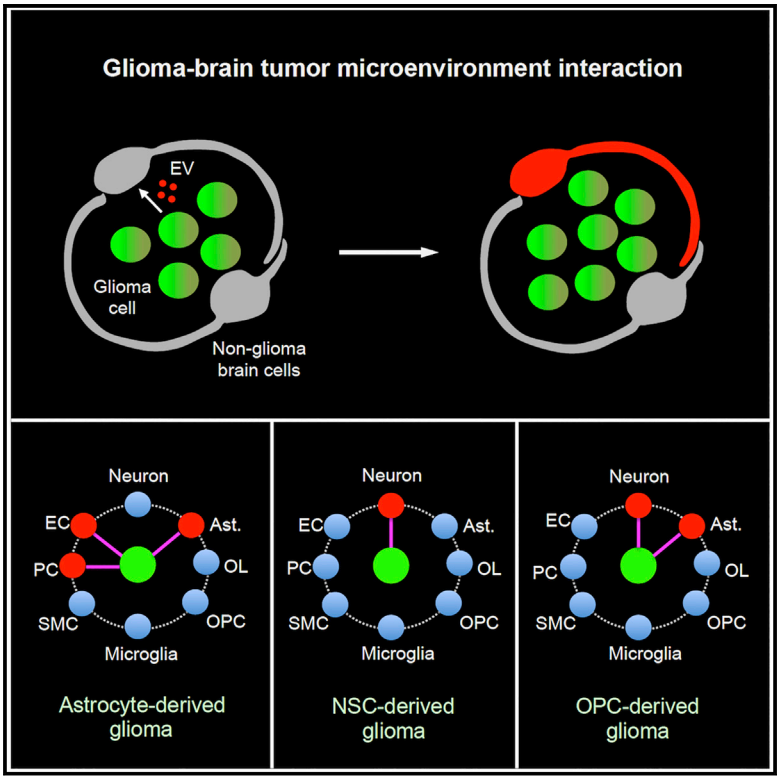


## Highlights

- Distinct types of gliomas interact with different sets of brain cells
- Glioma cells use extracellular vesicles to achieve the glioma-brain-cell crosstalk
- EV-mediated communication alters neuronal activity in the labeled neurons

## Authors

Xiaofei Gao, Zhaohuan Zhang, Tomoyuki Mashimo, ..., Wenzhi Sun, Robert M. Bachoo, Woo-ping Ge

## Correspondence

woo-ping.ge@utsouthwestern.edu

## In Brief

Non-glioma cells form a unique tumor microenvironment and are critical for glioma progression. Gao et al. find that individual gliomas communicate with distinct sets of non-glioma cells, including glial cells, neurons, and vascular cells. Transfer of genetic material is achieved mainly through extracellular vesicles (EVs).

Gao et al., 2020, Cell Reports *30*, 2489–2500
February 25, 2020
https://doi.org/10.1016/j.celrep.2020.01.089

Cell Reports
Report



# Gliomas Interact with Non-glioma Brain Cells via Extracellular Vesicles

Xiaofei Gao,[1] Zhaohuan Zhang,[1,2] Tomoyuki Mashimo,[3] Bo Shen,[1] James Nyagilo,[4] Hao Wang,[1] Yihui Wang,[1,5] Zhida Liu,[6] Aditi Mulgaonkar,[7] Xiao-Ling Hu,[1] Sara G.M. Piccirillo,[3] Ugur Eskiocak,[1] Digant P. Davé,[4,8] Song Qin,[9] Yongjie Yang,[10] Xiankai Sun,[7] Yang-Xin Fu,[6] Hui Zong,[11] Wenzhi Sun,[12,13] Robert M. Bachoo,[3,4,14] and Woo-ping Ge[1,4,14,15,16,*]

[1]Children's Research Institute and the Department of Pediatrics, University of Texas Southwestern Medical Center, Dallas, TX 75390, USA
[2]Department of Neurology, Changzheng Hospital, Second Military Medical University, Shanghai 200003, China
[3]Department of Internal Medicine, University of Texas Southwestern Medical Center, Dallas, TX 75390, USA
[4]Department of Neurology and Neurotherapeutics, University of Texas Southwestern Medical Center, Dallas, TX 75390, USA
[5]Tongji Hospital Tongji Medical College, Huazhong University of Science and Technology, Wuhan, Hubei 4300030, China
[6]Department of Pathology, University of Texas Southwestern Medical Center, Dallas, TX 75390, USA
[7]Department of Radiology, University of Texas Southwestern Medical Center, Dallas, TX 75390, USA
[8]Department of Bioengineering, University of Texas, Arlington, TX 76010, USA
[9]Department of Anatomy, Histology and Embryology, School of Basic Medical Sciences, Fudan University, Shanghai 200032, China
[10]Department of Neuroscience, Graduate School of Biomedical Sciences, Tufts University School of Medicine, Tufts University, Boston, MA 02111, USA
[11]Department of Microbiology, Immunology, and Cancer Biology, University of Virginia, Charlottesville, VA 22908, USA
[12]Chinese Institute for Brain Research, Beijing 102206, China
[13]School of Basic Medical Sciences, Capital Medical University, Beijing 100069, China
[14]Harold C. Simmons Comprehensive Cancer Center, University of Texas Southwestern Medical Center, Dallas, TX 75390, USA
[15]Department of Neuroscience, University of Texas Southwestern Medical Center, Dallas, TX 75390, USA
[16]Lead Contact
*Correspondence: woo-ping.ge@utsouthwestern.edu
https://doi.org/10.1016/j.celrep.2020.01.089

## SUMMARY

**Emerging evidence suggests that crosstalk between glioma cells and the brain microenvironment may influence brain tumor growth. To date, known reciprocal interactions among these cells have been limited to the release of paracrine factors. Combining a genetic strategy with longitudinal live imaging, we find that individual gliomas communicate with distinct sets of non-glioma cells, including glial cells, neurons, and vascular cells. Transfer of genetic material is achieved mainly through extracellular vesicles (EVs), although cell fusion also plays a minor role. We further demonstrate that EV-mediated communication leads to the increase of synaptic activity in neurons. Blocking EV release causes a reduction of glioma growth *in vivo*. Our findings indicate that EV-mediated interaction between glioma cells and non-glioma brain cells alters the tumor microenvironment and contributes to glioma development.**

## INTRODUCTION

The brain consists of multiple cell types that form a complex neuron–glia-blood vasculature network. During glioma development, glioma cells infiltrate normal brain tissue and interact with cells in this network (Charles et al., 2012; Fan, 2019). Glioma cells secrete many cytokines, growth factors, and chemokines that can alter the properties of various brain cells (Charles et al., 2012). As a result, these neighboring non-glioma brain cells form a unique tumor microenvironment (TME), which is critical for glioma progression (Calabrese et al., 2007; Gilbertson and Rich, 2007; Jain et al., 2007).

Neurons and glial cells in the TME can participate in glioma development through many mechanisms, including glia-derived growth factors (Heldin, 2013; Rath et al., 2013; Seike et al., 2011), metalloproteinases that facilitate glioma invasion (Le et al., 2003; Roth et al., 2010; Seike et al., 2011), pro-inflammatory cytokines (Coniglio and Segall, 2013; Li et al., 2010; Li and Graeber, 2012) involved in immunosuppression (e.g., transforming growth factor β [TGF-β]) (Coniglio and Segall, 2013; Seike et al., 2011), gap junctions (Aftab et al., 2015; Hong et al., 2015; Zhang et al., 1999), neuron-derived neuroligin-3 (Venkatesh et al., 2015, 2017), and activity from direct synaptic connections (Venkataramani et al., 2019; Venkatesh et al., 2019; Zeng et al., 2019). Recently, cancer cells were found to secrete extracellular vesicles (EVs; including exosomes) containing proteins, mRNA, and microRNA (miRNA) (Abels and Breakefield, 2016; Abels et al., 2019; Al-Nedawi et al., 2008; Gibbings et al., 2009; Graner et al., 2009; Skog et al., 2008). Due to their ability to transfer nucleic acids, proteins, and lipids, EVs are known to mediate intercellular communication for both normal cells and cancer cells (Gibbings et al., 2009; Lo Cicero et al., 2015).

The glioma microenvironment possesses a high level of heterogeneity (Charles et al., 2012). This complexity relies on network-based communication between many cell types,

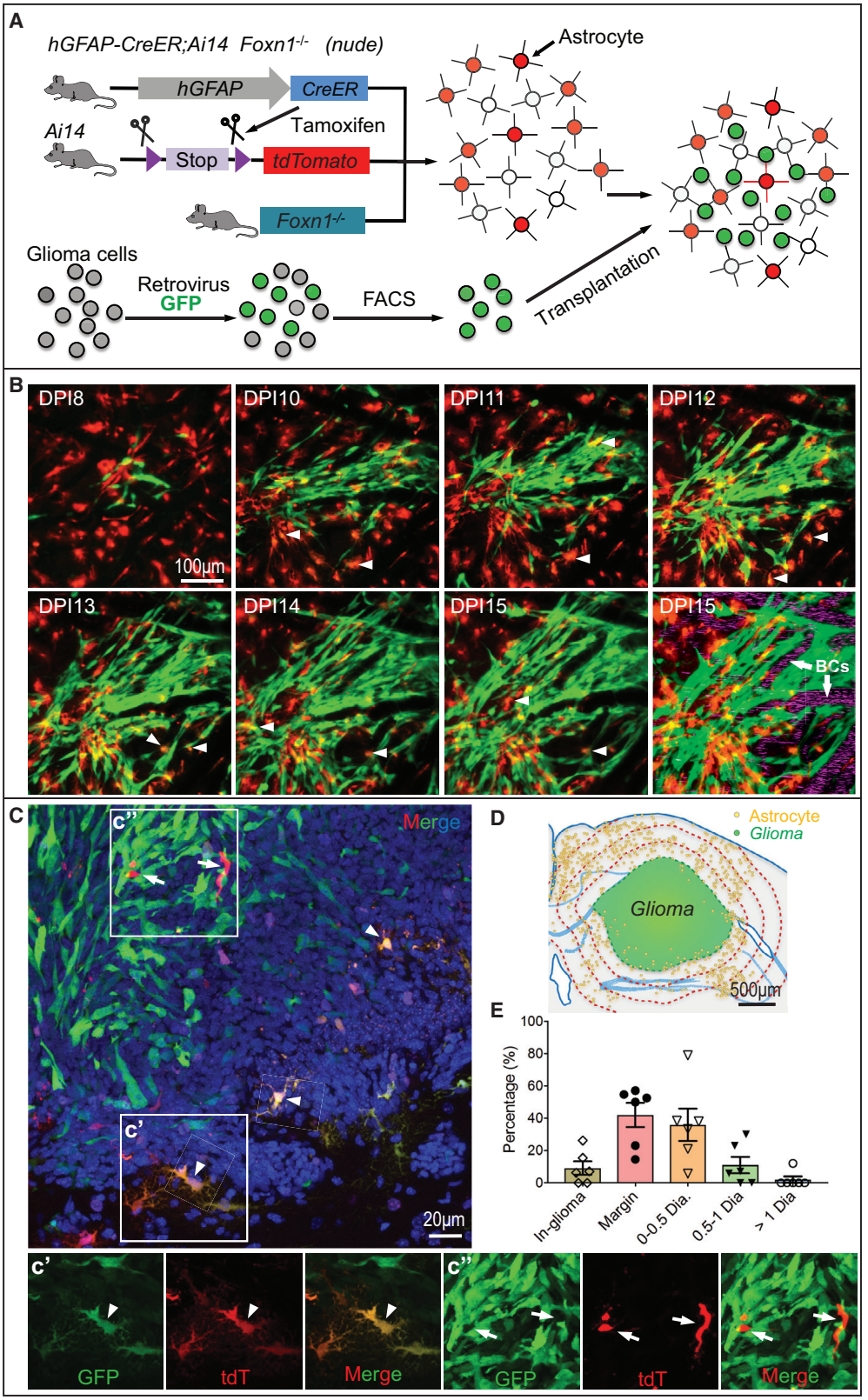


*(legend on next page)*

including the different glial cells, neurons, blood vascular cells, secreted factors, and surrounding matrix (Charles et al., 2012). EVs secreted by glioma cells are increasingly recognized in a number of processes underlying glioma progression, such as facilitating the transport of receptors, signaling molecules, oncogenic genes, and miRNAs (Abels and Breakefield, 2016; Gourlay et al., 2017; Nakano et al., 2015; Rajendran et al., 2014; Skog et al., 2008), thus contributing to the modification of the surrounding microenvironment (Godlewski et al., 2015). Improved understanding of the biology of glioma EVs and the glioma-glia interaction they mediate, as well as their roles in glioma progression, will provide a potential therapeutic target/delivery system. However, much is unknown about whether glioma cells actively communicate with non-glioma cells of the TME by EVs *in vivo* and whether altering the properties of the non-glioma cells by EVs creates a microenvironment for glioma growth. Each glioma has a distinct cellular origin and cellular properties (Alcantara Llaguno et al., 2009; Assanah et al., 2006; Bachoo et al., 2002; Lindberg et al., 2009; Liu et al., 2011; Louis et al., 2016; Persson et al., 2010; Singh et al., 2004; Verhaak et al., 2010; Visvader, 2011; Wang et al., 2009; Zhu et al., 2005). To date, it is unclear whether a particular glioma cell type prefers to communicate with a specific set of non-glioma cells in the brain or whether all gliomas, although distinct, communicate non-specifically with the same set of brain cells.

The main challenge in studying interactions between glioma cells and non-glioma brain cells *in vivo* is to clearly distinguish these two cell types and directly characterize their interactions *in vivo* for days to weeks during glioma development. By developing triply transgenic nude mice to label both cell types with fluorescent proteins, we provided a dynamic picture of the interactions between glioma cells and adjacent glia/neurons/vascular cells in the brain with longitudinal time-lapse imaging technology. Our results delineated how gliomas alter gene expression in distinct brain cells and elucidated the role of EV-mediated communication in alteration of non-glioma cell properties and glioma growth.

## RESULTS

### Time-Lapse Imaging of the Interaction between Glioma Cells and Astrocytes

To image glioma cell behavior *in vivo*, especially in deep cortical layers, it is crucial to establish stable glioma cell lines tagged with fluorescent proteins. We have produced mouse glioma cell lines that express green fluorescent protein (GFP) for *in vivo* imaging, including the astrocyte-derived glioma cell line 73C (*BRAF$^{V600E}$;Pten$^{-/-}$;p53$^{-/-}$*, see the details in STAR Methods). After fluorescence-activated cell sorting, 73C cells stably expressed GFP even when cultured for 2 months (Figure S1A). Upon transplantation into *Foxn1$^{nu}$* (*Foxn1$^{-/-}$*, nude background) and C57BL/6J mice, all of the mice developed gliomas (>2 mm in diameter) in 2–4 weeks (Figure S1B).

Glial cells constitute 50% of the cells in the human brain and are critical for brain metabolism, neuronal protection, and cell-cell interactions (Iadecola and Nedergaard, 2007; Molofsky et al., 2012; Patel et al., 2014). Astrocytes are the largest glial population associated with gliomas. To observe astrocytes *in vivo* and analyze glioma-astrocyte interactions, we established the stable mouse strain *hGFAP-CreER;Ai14;Foxn1$^{-/-}$* to genetically tag astrocytes with tdTomato (Figure 1A; Figures S1C and S1D) so we could image the morphology and dynamics of astrocytes and analyze their interactions with GFP-expressing gliomas. In different brain regions except the neurogenic regions, crossing *hGFAP-CreER* mice with *Ai14* mice to generate *hGFAP-CreER;Ai14* allowed robust expression of tdTomato uniquely in astrocytes after we administered tamoxifen to these mice as adults (>P50) (Casper et al., 2007). Astrocyte morphology and distribution from *hGFAP-CreER;Ai14;Foxn1$^{-/-}$* mice were not noticeably different than in those from *hGFAP-CreER;Ai14;Foxn1$^{+/-}$* mice (Figure S2A). We transplanted GFP$^+$ glioma cells into the brains of *hGFAP-CreER;Ai14;Foxn1$^{-/-}$* mice. Beginning at 8 days post-injection (DPI), we began to observe GFP$^+$ glioma cells in the imaging field visible through a cranial window (Figure 1B). Interestingly, we observed multiple cells with both GFP and tdTomato expression within the field at around 10 DPI. More double-labeled cells appeared in the following week (Figure 1B). These cells had typical astrocyte morphology (Figure 1C). This indicated that astrocytes likely obtained GFP (protein, mRNA, or DNA) from glioma cells. Most of these cells (tdTomato$^+$GFP$^+$; i.e., double-labeled astrocytes) were located near the 73C gliomas (Figure 1D). However, a substantial portion of double-labeled astrocytes were >400 μm away from the glioma mass (38.26%, n = 246 of 643 cells; Figure 1D; Figure S1D). Most of the double-labeled astrocytes were located in the glioma margin and the region close to the glioma margin. However, there was lower density of labeled astrocytes inside the gliomas themselves (Figure 1E), indicating that glioma-astrocyte interactions might not be mediated by direct cell-cell contact, but we cannot exclude the possibility that some glioma cells actively migrated into the region far away from the glioma mass and directly contacted non-glioma brain cells. In addition, we

**Figure 1. *In Vivo* Imaging of Glioma-Glia Interactions**

(A) The strategy for studying interactions between astrocytes and glioma cells in the brain. Glioma cells were infected with retrovirus-GFP and then transplanted into the brains of *hGFAP-CreER;Ai14;Foxn1$^{-/-}$* mice.

(B) Live imaging of glioma development. DPI, days post-injection of glioma cells; red, tdTomato$^+$ astrocytes; green, GFP$^+$ 73C glioma cells; purple, pseudo-color of blood cells (BCs) labeled with DiD at 15 DPI.

(C) Staining of the brain section from a *hGFAP-CreER;Ai14;Foxn1$^{-/-}$* mouse with GFP$^+$ 73C glioma cells. The yellow cells (tdTomato$^+$GFP$^+$) showed astrocytic morphology (arrowheads). c' and c'', insets from c. Blue, nucleus stained with Hoechst 33342.

(D) Distribution of yellow astrocytes (tdTomato$^+$GFP$^+$) in a brain section. Green, glioma with GFP$^+$ glioma cells. The distance between each pair of dashed lines is 200 μm.

(E) The density of yellow astrocytes (tdTomato$^+$GFP$^+$) located in the inside of the glioma mass or far away from it (inside glioma, 9.19% ± 4.53%; margin, −50 μm to +50 μm from the tumor edge, 42.04% ± 8.19%; 0–0.5 glioma diameter, 35.96% ± 10.98%; 0.5–1 diameter, 11.05% ± 5.61%; >1 diameter, 2.02%+2.21%; n = 6 mice).

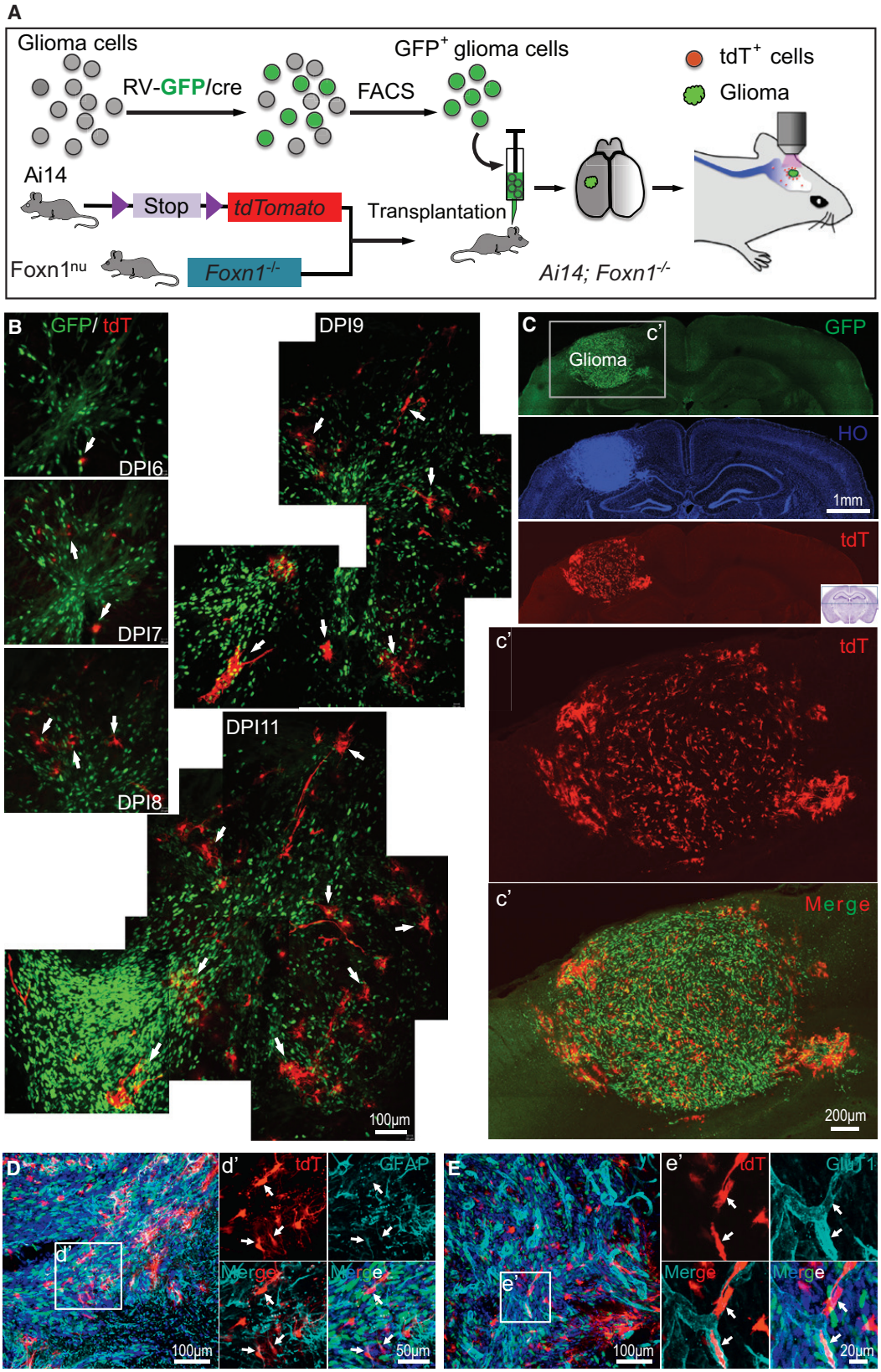


*(legend on next page)*

observed that GFP$^+$tdTomato$^+$ astrocytes near gliomas had a hypertrophic morphology of reactive astrocytes in the brains of *hGFAP-CreER;Ai14* mice with GFP-73C gliomas. The astrocyte-covered area around gliomas was significantly larger than in a control region (control region in contra-hemisphere, 1,124.4 ± 42.6 $\mu m^2$, n = 45; control region in ipsi-hemisphere, 1,146.7 ± 39.3 $\mu m^2$, n = 21; glioma margin, 1,930.9 ± 66.4 $\mu m^2$; n = 30 astrocytes; Figures S2B–S2G).

## Time-Lapse Imaging of Glioma-Brain Cell Communication

To test whether astrocytes are the only cell type in the brain with which 73C gliomas interact, we used the Cre/LoxP system to report cell-cell communications, as previously used in mammary tumor cells and melanoma cells (Zomer et al., 2015). Combining this method with longitudinal time-lapse live imaging, we were able to directly observe how GFP/cre-expressing 73C glioma cells interact with brain non-glioma cells in *Ai14;Foxn1*$^{-/-}$ mice (Figures 2A–2C). We transplanted 5,000–10,000 GFP/cre-expressing 73C glioma cells into the brains of *Ai14;Foxn1*$^{-/-}$ mice. Surprisingly, we started to observe tdTomato$^+$ cells at 6 DPI (Figures 2B and 2C). The number of tdTomato$^+$ cells increased dramatically within the second week post-transplantation. At 9 DPI, the density of tdTomato$^+$ cells reached a plateau. Most of these tdTomato$^+$ cells had glial cell morphology (Figure 2B). These data indicated that Cre recombinase from the 73C cells was able to recombine the conditional tdTomato reporter in the host brain cells (i.e., by removing the stop codon between the loxP sequences in nearby non-glioma cells).

## Characterization of Brain Cell Types That Interacted with 73C Glioma Cells

To further investigate whether astrocytes were the only cell type that received GFP/cre from 73C glioma cells, we stained brain sections with anti-GFAP for astrocytes, anti-NeuN for neurons, aniti-Iba1 for microglial cells and macrophages, anti-NG2 for NG2 glial cells (i.e., OPCs [oligodendrocyte precursor cells]), anti-PDGFRb for pericytes and anti-GluT1 or anti-CD31 for endothelial cells to determine the identities of the tdTomato$^+$ cells. We demonstrated that half of these tdTomato$^+$ cells had astrocytic morphology and were GFAP$^+$ (49.45% ± 4.20%, n = 6 mice; Figure 2D), indicating that 73C-GFP/cre glioma cells transferred Cre mainly to astrocytes. We also found that a notable number of tdTomato$^+$ cells were also GluT1$^+$, indicating that they were endothelial cells (27.31% ± 6.80%, n = 6 mice, Figure 2E). In addition, we transplanted 73C-GFP/cre glioma cells into *Ai14* mice with the C57BL/6J background. Although BRAF$^{V600E}$ is rare in adult patients (Brennan et al., 2013), nearly half of pediatric patients with high-grade gliomas or transformed gliomas have this mutation (Mistry et al., 2015). As we observed in *Ai14;Foxn1*$^{-/-}$ mice, 73C gliomas also induced tdTomato expression in astrocytes and vascular cells in immunocompetent *Ai14* mice (data not shown).

## Distinct Types of Gliomas Interact with Different Sets of Brain Cells

To assess whether distinct types of gliomas interact with unique sets of brain cells, we used three different glioma cell lines that represent three different glioma cell types: astrocyte-derived 73C (*BRAF*$^{V600E}$*;Pten*$^{-/-}$*;p53*$^{-/-}$), neural-stem-cell–derived PS5A (*Ink4a*$^{-/-}$*Pten*$^{-/-}$*Egfr*$_{VIII}$) (Singh et al., 2017), and OPC–derived OPC-HZ (*p53*$^{-/-}$*NF1*$^{-/-}$) (Liu et al., 2011) (see details in STAR Methods). The tumors produced from these cell lines in the brain were quite distinct, as evidenced by their electrophysiological properties and their distribution in the brain (Figures 3A–3C; Figure S3). Both PS5A and OPC-HZ cells lines formed large tumor masses ~1 month after transplantation of 10,000 cells into NOD-*scid IL2rg*$^{null}$ (NSG) mice (Figures S3A and S3B). 73C cells showed astrocyte-like ion channel properties. Their current-voltage characteristic curves (I-V curves) were passive and linear. PS5A and OPC-HZ glioma cells demonstrated typical type A transient potassium channel ($K_a$) and delayed rectifier potassium channel ($K_d$) currents (Figures 3A–3C). Their distribution patterns in the brain were notably different after transplantation (Figures 2C, 3D, and 3G; Figures S1B, S1D, and S3). 73C glioma cells consistently formed a tumor mass and penetrated normal brain tissue along blood vessels (Figures 1D and 2E; Figure S3C). PS5A glioma cells did not form a dense cell mass and were sparsely distributed in the brain in the early stage of tumor formation (Figure 3D and Figure S3C). OPC-HZ cells formed a tumor with an intermediate density, lower than that of 73C cells but higher than that of PS5A cells (Figure 3G; Figure S3). After we transplanted these different GFP/cre-expressing glioma cells into the brains of *Ai14* and *Ai14;Foxn1*$^{-/-}$ mice, interestingly, we observed, unlike GFP/cre-expressing 73C glioma cells, that PS5A glioma cells (infected with RV-GFP/cre) transferred Cre mainly to neurons (83.54% ± 5.84%; i.e., NeuN$^+$tdTomato$^+$cells/all tdTomato$^+$ cells), a few astrocytes (5.57% ± 1.40%; i.e., GFAP$^+$ tdTomato$^+$ cells/all tdTomato$^+$ cells), and a few microglia (3.58% ± 2.195%, n = 5 mice; i.e., Iba-1$^+$ tdTomato$^+$ cells/all tdTomato$^+$ cells; Figure S4); Among these neurons, a small portion were GABAergic neurons (28.9% ± 4.1%, n = 4); no vascular cells with tdTomato expression were observed (i.e., GluT1$^+$ tdTomato$^+$ cells/all tdTomato$^+$ cells; Figures 3D–3F and 3J). GFP/cre-expressing OPC-HZ cells derived from oligodendrocyte precursors transferred Cre mainly to neurons (63.29% ± 12.90%) and to astrocytes (14.28% ± 4.98%) but to very few microglia (0.88% ± 0.88%, n = 5 mice; Figures 3G–3J).

**Figure 2. Gliomas Alter the Chromosomal DNA of Adjacent Brain Cells**

(A) The strategy for studying the interactions of GFP/cre-expressing glioma cells and brain cells in *Ai14;Foxn1*$^{-/-}$ mice.

(B) Time-lapse live imaging of the appearance of tdTomato$^+$ cells (red, arrows) after transplantion of GFP/cre-expressing 73C glioma cells into an *Ai14;Foxn1*$^{-/-}$ mouse. The number of both glioma cells and tdTomato-expressing cells (red) gradually increased in the following week.

(C) Image of a brain section from an *Ai14;Foxn1*$^{-/-}$ mouse with GFP/cre-expressing glioma. Green, glioma cells with GFP/cre expression; blue, nuclei stained with Hoechst 33342 (HO); red, brain cells with tdTomato expression (tdT). c', inset.

(D and E) Staining of brain sections for astrocytes (D) (arrows, GFAP, light blue, pseudo-color of Alexa 647) and endothelial cells (E) (arrows, GluT1, light blue, pseudo-color of Alexa 647). d' and e', insets from (D) and (E), respectively.

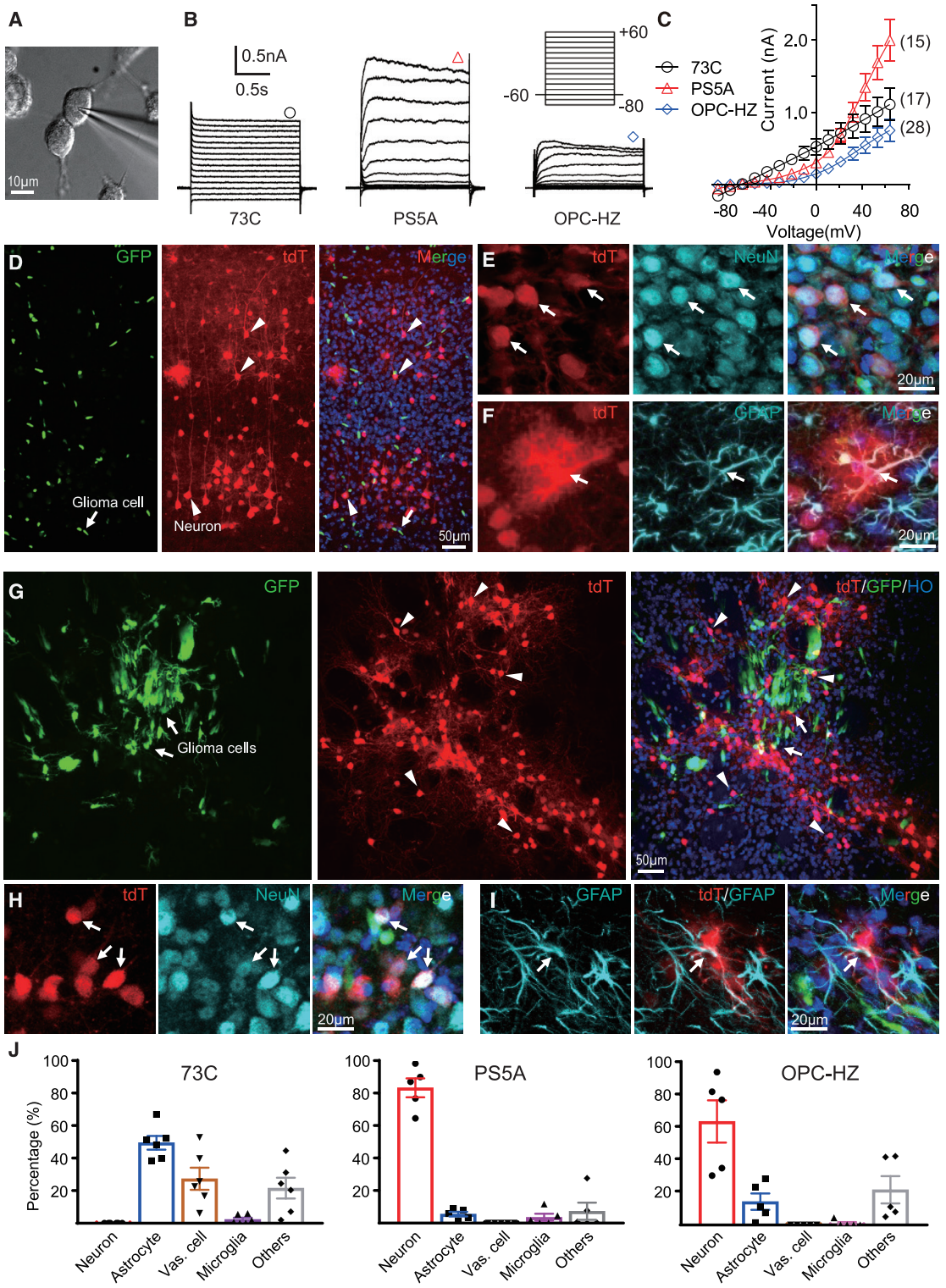


**Figure 3. Distinct Gliomas Interact with Distinct Sets of Brain Cells**

(A–C) Whole-cell recording of glioma cells of different origins *in vitro* (A). Currents from 73C, PS5A, and OPC-HZ cells were obtained with hyperpolarized and depolarized voltage stimuli (from −80 to +60 mV; duration, 2 s; holding potential, −60 mV) (B). Their I-V curves are shown in (C).

*(legend continued on next page)*

### Alteration of Properties of Neurons Obtaining EVs from Glioma Cells

To determine whether EV-mediated communication alters properties of non-glioma brain cells, we performed whole-cell recording and compared the intrinsic properties and synaptic activity of neurons from *Ai14* tg mice with glioma cells (Figure 4A). We transplanted GFP/cre-expressing PS5A glioma cells into *Ai14* mouse brains and recorded labeled neurons (which received EVs from glioma cells) and their neighbors (i.e., unlabeled neurons that were very close to these labeled neurons). A significant difference was observed in the synaptic activity between labeled and unlabeled neurons (Figures 4B–4H). Labeled neurons had a higher frequency of spontaneous synaptic response (Figure 4C), but their amplitudes showed no obvious difference (Figures 4F–4H), indicating that the EV-mediated communication altered neuronal activity in the labeled neurons. It has been reported that activity-dependent neuron-derived Neuroligin-3 contributes to glioma growth (Venkatesh et al., 2015, 2017). How this alteration of neuronal activity in our case might affect tumor growth or progression requires further intense investigation in the future.

### Glioma-Brain Cell Communication Mediated by Cell Fusion

Cell fusion has been reported in numerous tumor cell types, between tumor cells, or between tumorigenic cells, and normal cells might contribute to tumor progression (Bjerkvig et al., 2005). To investigate the contribution of cell fusion to glioma-brain cell communication, we analyzed cells with green nuclei and red cytoplasm in brain sections after glioma transplantation. Because GFP/cre has a nuclear localization signal peptide, it is expressed predominantly in the nucleus. If cell fusion was occurring between individual glioma cells and adjacent brain cells, we should be able to detect very bright green nuclei in tdTomato$^+$ cells. We revealed a very low percentage (73C, ~1.20% ± 0.68%, n = 5) of tdTomato$^+$ cells with bright green nuclei at 14 DPI (Figures 5A and 5B), indicating a very low number of fusion events between glioma cells and adjacent non-glioma brain cells, which is consistent with a previous report in other cancer cells (Zomer et al., 2015). In addition, we observed that the numbers of tdTomato$^+$ cells arising from cell fusion in PS5A and OPC-HZ gliomas were also very low (PS5A, 1.63% ± 0.48%, n = 5; OPC-HZ, 0.06% ± 0.06%, n = 5; Figure 5B). These results are also consistent with our observations from an analysis with flow cytometry (Figures 5C and 5D).

### Glioma-Brain Cell Communication Mediated by EVs

EVs including exosomes contain distinct subsets of RNAs and proteins (Lo Cicero et al., 2015; Skog et al., 2008; Valadi et al., 2007; Zhu, 2019). We observed vesicles being shed by both human and mouse glioma cells *in vitro* (Video S1; Figure 5E). To determine whether EVs purified from glioma cells contained Cre mRNA, we cultured 73C glioma cells *in vitro* and purified EVs as previously reported (Lässer et al., 2012; Skog et al., 2008). We observed that Cre and GFP mRNAs were present in purified EVs from cultured GFP/cre- or GFP-expressing 73C glioma cells (Figure 5F), which indicated that EVs transport Cre and GFP mRNA. To characterize the EVs, we measured their size distribution using electron microscopy (EM) and the dynamic laser scattering (DLS) technique (Figures 5G–5I). We observed EVs with a size distribution from 40 to 200 nm (the media was filtered with 220-nm filters during EV preparation). The average diameter of these EVs from EM was 96.19 ± 0.73 nm (n = 3,977 EVs), which is similar to the size that we obtained with the DLS technique (98.03 ± 12.26 nm, n = 5 measurements; Figure 5J). CD63 is a specific membrane protein of EVs (Escola et al., 1998). To label EVs in cells, we infected 73C glioma cells with lentivirus (LV)-CD63-GFP, which we used for labeling the EV membrane, as previously reported (Men et al., 2019). After co-culturing these glioma cells in transwells with primary astrocytes below the transwells (Figure S5), we detected GFP$^+$ EVs from astrocytes. These results indicate that glioma-derived EVs were released into the media and then were received by the astrocytes (Figure S5).

We then injected purified EVs (1 μl) derived from GFP/cre-expressing 73C glioma cells into one hemisphere of the brains of *Ai14;Foxn1*$^{-/-}$ or *Ai14* mice (i.e., C57BL/6J background). As a control, EVs from GFP-expressing 73C glioma cells were injected into the contralateral hemisphere of the same animal (Figure 5K). We detected tdTomato$^+$ cells in brain sections at 8 DPI, with the tdTomato$^+$ cells showing astrocyte morphology and possessing endfeet with blood vessels. Additional staining confirmed that around half of the tdTomato$^+$ cells were astrocytes (Figures 5L and 5M). These results strongly indicated that EVs are able to transport Cre mRNA and protein into astrocytes. To test the contribution of EV-mediated communication in glioma growth, we used a LV with a short hairpin RNA (shRNA) targeting Rab27a, a mediator of EV secretion, as described in previous studies (Zhang et al., 2015). We observed that 73C glioma cells with *LV-Rab27a-shRNA* infection produced significantly smaller gliomas than those infected with control LV (Figures 5P, and 5Q). To exclude the possibility that Rab27a has a cell-autonomous effect on glioma growth, we infected glioma cells with *LV-Rab27a-shRNA* and LVs with scrambled controls. We observed that *Rab27a-shRNA* had an effect on glioma cell growth. The density of 73C glioma cells in the Rab27a shRNA group was 53.8% of that in control group (control, 2,661.5 ± 273.5 cells/mm$^2$; *Rab27a-shRNA*, 1,431.6 ± 121.3 cells/mm$^2$;

(D–F) GFP/cre-expressing PS5A glioma cells were transplanted into *Ai14;Foxn1*$^{-/-}$ mice. Most tdTomato$^+$ cells exhibited neuronal morphology (D) (arrowhead). A few astrocytes in the cerebral cortex displayed a bushy morphology. Green, nuclei of GFP/cre-expressing glioma cells (arrow); blue, nuclei (Hoechst 33342); anti-NeuN, neuron (E) (arrows); anti-GFAP, astrocyte (F) (arrows).

(G) GFP/cre-expressing OPC-HZ glioma cells (arrows, note OPC-HZ cells had GFP expression also in the cytoplasm) were transplanted into *Ai14;Foxn1*$^{-/-}$ mice. Most tdTomato$^+$ cells showed neuronal morphology (arrowheads).

(H and I) Brain sections from these mice in (G) were labeled with anti-NeuN (H) (neurons, arrows) and anti-GFAP (I) (astrocytes, arrows).

(J) Percentages of different kinds of brain cells (neurons, astrocytes, microglia, vascular cells, and others) among all tdTomato-expressing cells in *Ai14;Foxn1*$^{-/-}$ mice with transplantation of three different GFP/cre-expressing glioma cells (73C, PS5A, and OPC-HZ; n = 5 mice for each group). Blue signals in (D–I), Hoechst 33342 (HO).

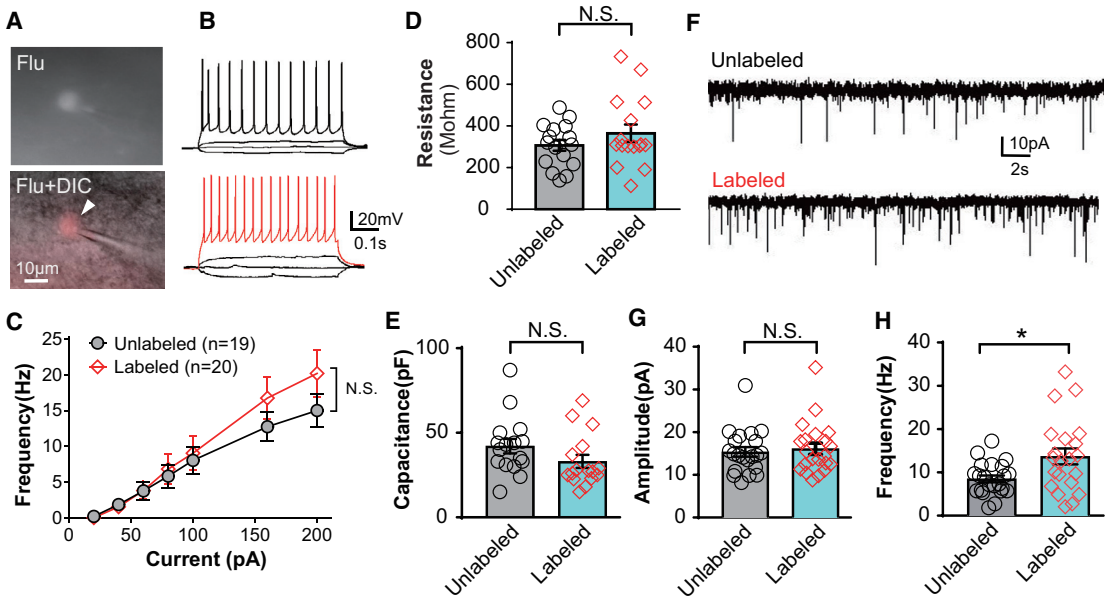


**Figure 4. Electrophysiological Properties of Neurons with and without Receipt of EVs from Glioma Cells**

(A) Labeled neurons and their neighbors (i.e., unlabeled neurons that were very close to these labeled neurons) were recorded in *Ai14* mouse brains 3 weeks after GFP-Cre-expressing PS5A glioma cells were transplanted.

(B–E) Action potential firing pattern (B and C) and cell membrane properties (D and E) recorded from labeled and unlabeled neurons in the cerebral cortex.

(F–H) Spontaneous synaptic activity was measured. (F) Example traces of spontaneous postsynaptic responses recorded in labeled and neighboring unlabeled neurons. Summarized results of amplitude (unlabeled, 15.37 ± 1.11 pA, n = 21; labeled, 16.11 ± 1.33 pA, n = 21) (G) and frequency (unlabeled, 8.49 ± 0.80 Hz, n = 22; labeled, 13.69 ± 1.85 Hz, n = 21) (H) of spontaneous postsynaptic responses recorded from labeled and unlabeled neurons. *p < 0.05; two-tailed unpaired t test. All error bars indicate SEM.

Figure 5O). Interestingly, the volumes of gliomas with *Rab27a* shRNA were only about 1/30 (i.e., 3.25%) of the size of those of the control group (control, 3.65 ± 0.39 $mm^3$; *Rab27a*-shRNA, 0.12 ± 0.05 $mm^3$), indicating knockdown of Rab27a may play a role in the inhibition of glioma growth.

## DISCUSSION

Previous studies on glioma-microenvironment interactions have usually involved fixed brain tissues or *in vitro* model systems; such studies have mainly focused on astrocyte-derived growth factors and metalloproteinases that facilitate glioma invasion, pro-inflammatory cytokines involved in immunosuppression (e.g., TGF-β), or gap junctions (Calabrese et al., 2007; Charles et al., 2012; Gilbertson and Rich, 2007; Jain et al., 2007). Our observations delineate how gliomas can horizontally transfer genetic material or directly transfer protein (by EVs or cell fusion) to alter gene expression in distinct non-glioma brain cells and provide a dynamic picture of the interactions between glioma cells and adjacent non-glioma brain cells with longitudinal time-lapse imaging.

Determining how cells from individual gliomas interact with normal brain cells is a fundamental issue in brain tumor research (Charles et al., 2012; Placone et al., 2016). Although we know that astrocytes and cancer cells can exchange miRNAs or non-coding RNAs through EVs (Zhang et al., 2015) or by gap junctions (Li et al., 2013), much is unclear about the pathway involved in the response of reactive astrocytes during glioma development (Charles et al., 2012; Placone et al., 2016). In our study, glioma cells altered the chromosomal DNA of adjacent brain cells, which could be mediated through two potential means, i.e., by cell fusion or EVs. We do not, however, exclude other possibilities, e.g., possibly microtubes, which have been reported to allow multicellular communication among astrocytoma cells (Osswald et al., 2015). Hematopoietic cells releasing mRNAs and miRNAs by EVs can be absorbed by neurons (Ridder et al., 2014). It was also reported that exosomes released from brain cancer cells fuse with brain endothelial cells (Hoshino et al., 2015).

Because *Rab27a-shRNA* has a cell-autonomous effect on cell growth, we cannot exclude the possibility that the inhibition of tumor growth observed *in vivo* (1/30 of control gliomas) might be partially due to a cell-autonomous effect, although the tumor growth *in vivo* was inhibited by over 95% and showed a larger effect than was seen *in vitro* (~50%).

EVs secreted by glioma cells are increasingly recognized as having a role in a number of processes underlying glioma progression (Godlewski et al., 2015; Gourlay et al., 2017; Nakano et al., 2015; Skog et al., 2008). They are emerging as a key component in the biogenesis of gliomas, in addition to contributing to the modification of the surrounding microenvironment to influence glioma progression (Nakano et al., 2015). Different gliomas exchanged EVs with different sets of brain cell types, which might exclude non-specific communication between gliomas and brain cells because debris was preferentially taken up by astrocytes or microglia/macrophages. We also purified EVs from human glioma cells and injected them into the brains of *Ai14* mice (nude background). Interestingly, we did not detect

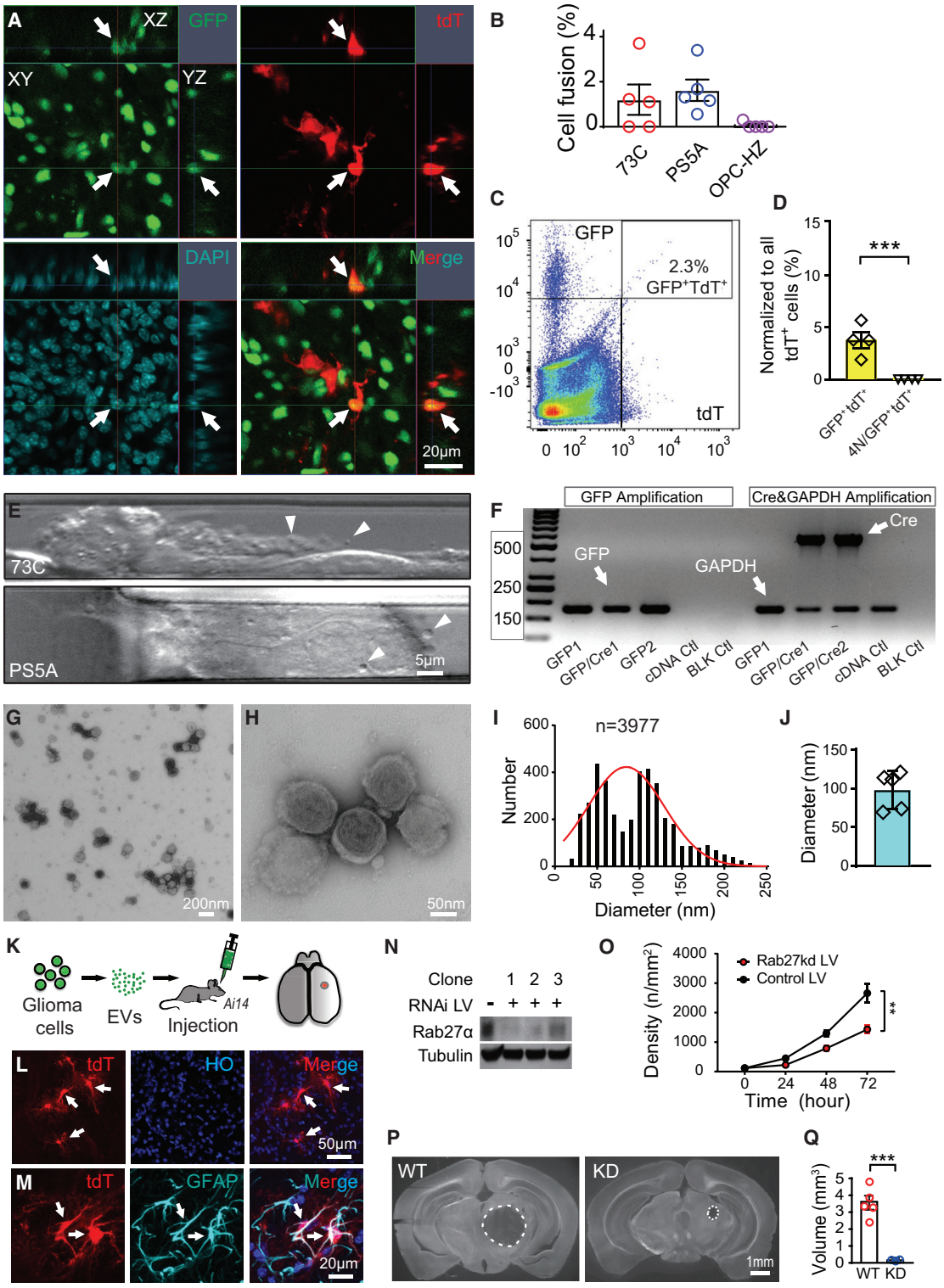


**Figure 5. Glioma-Non-glioma Cell Interactions Are Mediated by Cell Fusion and EVs**

(A) An example of the fusion of a tdTomato$^+$ astrocyte and a GFP/cre-expressing glioma cell (arrows).

(B) Summary of the percentage of fused cells (i.e., glioma cells and astrocytes) among all yellow cells after transplantation of three glioma cell lines.

(C and D) Fused tdTomato$^+$ cells were analyzed by flow cytometry. An example (C) and the summarized results (D) are shown. The fused tdTomato$^+$ cells were shown with 4N DNA among these tdTomato$^+$GFP$^+$ cells (i.e., 4N of 4′,6-diamidino-2-phenylindole [DAPI] signal).

*(legend continued on next page)*

any tdTomato cells in the brains (data not shown), which indicates the communication has cell-type specificity. Properties of normal cells might change dramatically near a tumor through this unique crosstalk. We demonstrated for the first time that EV-mediated communication leads to increased synaptic activity in neurons. These distinct interactions may also provide distinct targets for inhibiting the growth of these different gliomas. Understanding the biology of glioma EVs and the mechanism(s) by which they mediate the glioma-microenvironment interaction, as well as their roles in glioma development, will lead to new potential therapeutic targets for human brain tumors.

## STAR★METHODS

Detailed methods are provided in the online version of this paper and include the following:

- KEY RESOURCES TABLE
- LEAD CONTACT AND MATERIALS AVAILABILITY
- EXPERIMENTAL MODEL AND SUBJECT DETAILS
- METHOD DETAILS
  - Animals
  - Glioma cell lines
  - Glioma cell culture
  - Purification of retroviruses and *in vitro* infection of glioma cells
  - Cell sorting by flow cytometery
  - Purification of EVs
  - Glioma cell transplantation and EV injection
  - Blood cell labeling
  - Mouse thinned-skull and opened-skull preparations
  - Longitudinal time-lapse imaging *in vivo*
  - Immunostaining
  - Reverse transcription polymerase chain reaction (RT-PCR)
  - Whole-cell recording of glioma cells
  - Whole-cell recording of neurons in brain slices
  - Microfluidic channel imaging
  - Cell fusion analysis with flow cytometery
  - Imaging EVs with Electron Microscopy
  - Evaluation of 73C cell growth with or without knockdown of Rab27a
  - Transwell test of EV uptake by primary cultured astrocytes
- QUANTIFICATION AND STATISTICAL ANALYSIS
- DATA AND CODE AVAILABILITY

## SUPPLEMENTAL INFORMATION

Supplemental Information can be found online at https://doi.org/10.1016/j.celrep.2020.01.089.

## ACKNOWLEDGMENTS

We thank C. Liu, Z.-L. Wang, and Children's Research Institute (CRI) colleagues S.J. Morrison, J. Xu, R. Deberardinis, H. Zhu, and P. Mishira for advice on the project; J.-M. Jia for advice on live imaging; R. Jackson, A. Darehshouri, and K. Luby-Phelps from the University of Texas Southwestern Medical Center (UTSW) Electron Microscopy Core Facility for imaging extracellular vesicles with electron microscopy; Y.-X. Sun for advice on glioma cell culture; and B. Samuels, H. Zhao, N.N. Lu, J. Hu, and L.-J. Wu for critical discussion and reading of the manuscript. This work is supported by the National Institute of Neurological Disorders and Stroke (NINDS) R01 (R01NS104009), Jonesville Foundation for Pediatric Cancer, University of Texas Southwestern High Impact/High Risk funds, NINDS K99/R00 (R00NS073735), and CRI start-up funds to W.-p.G.; National Institues of Health (NIH) grant R01NS065195 and Simmons Cancer Center NIH support grant 5P30CA142543 for R.M.B.; National Cancer Institute (NCI) grant R01-CA136495 to H.Z.; NCI grant CA141975; the CPRIT (RR150072) to Y.-X.F.; National Natural Science Foundation of China (no. 31871477) and National Key Basic Research Program of China (973 Program, no. 2014CB965001) to S.Q.; the Cary Council—Southwestern Medical Foundation Award to S.G.M.P.; the Hamon Center for Regenerative Science and Medicine Awards for X.G.; Ruth L. Kirschstein National Research Service Award (NRSA) Postdoctoral Fellowship (F32) from NHLBI (1F32HL139016-01) to B.S.; and an NINDS Pathway to Independence Award and the Dan Adams Thinking Outside the Box Award (from The Henrietta B. and Frederick H. Bugher Foundation) to W.-p.G.

## AUTHOR CONTRIBUTIONS

W.-p.G., X.G., and Z.Z. conceived the project. W.-p.G., X.G., Z.Z., and R.W.B. designed the experiments. X.G. performed all *in vivo* imaging experiments. X.G., Z.Z., H.W., and W.-p.G. completed most of the animal experiments and data analysis. W.S. assisted in designing and developing longitudinal live imaging. S.G.M.P., H.W., and T.M. prepared most of the glioma cells. B.S. and U.E. performed fluorescence-activated cell sorting. J.N. performed microfluidic channel imaging. A.M. and Z.L. measured EV size. W.-p.G., R.W.B., S.Q., Y.-X.F., X.S., Y.Y., and H.Z. provided reagents, cells, and animals. W.-p.G. and X.G. completed electrophysiological recordings. W.-p.G. and X.G. wrote the manuscript. All authors reviewed and edited the manuscript.

## DECLARATION OF INTERESTS

The authors declare no competing interests.

Received: March 4, 2019
Revised: September 22, 2019
Accepted: January 24, 2020
Published: February 25, 2020

(E) Example images of 73C and PS5A demonstrate that these glioma cells shed vesicles as they migrated through a microfluidic device.
(F) RT-PCR of Cre and GFP from the mRNA purified from EVs. GFP1, GFP2, GFP/cre1, and GFP/cre2 were cDNA samples from EVs purified from GFP-expressing 73C or GFP/cre-expressing 73C cells. cDNA ctl was from 73C-cells without GFP or GFP/cre. BLK ctl was a blank control with water.
(G–J) Characterization of EVs purified from 73C glioma cells. (G–I) The images and diameter distribution of EVs from scanned EM images. (J) EV size measured with the dynamic laser scattering (DLS) technique.
(K) The strategy for assessing EV-mediated alteration of chromosomal DNA in *Ai14;Foxn1*$^{-/-}$ mice.
(L) TdTomato$^{+}$ cells (red, arrows) observed in the cortical region 8 DPI of EVs purified from cultured GFP/cre-expressing 73C glioma cells.
(M) Astrocytes (arrows) were labeled with the antibody against GFAP. Light sky blue, GFAP (pseudo-color of Alexa 647); blue in (L) and (M), nuclei stained with HO.
(N–Q) Blockage of EV release from 73C glioma cells with *LV-Rab27a-shRNA* and its effect on glioma growth. (N) Western blot of Rab27a protein of 73C cell colonies with Rab27a shRNA and control selected by puromycin. (O) Density of 73C glioma cells with infection of scrambled RNA and Rab27a shRNA. (P) Example images of 73C gliomas from mice with and without Rab27a shRNA knockdown, respectively. (Q) Summarized results of volumes of gliomas with and without Rab27a knockdown in (P). ***$p < 0.001$; **$p < 0.01$; two-tailed unpaired t test. All error bars indicate SEM.

## REFERENCES


Abels, E.R., and Breakefield, X.O. (2016). Introduction to Extracellular Vesicles: Biogenesis, RNA Cargo Selection, Content, Release, and Uptake. Cell. Mol. Neurobiol. *36*, 301–312.

Abels, E.R., Maas, S.L.N., Nieland, L., Wei, Z., Cheah, P.S., Tai, E., Kolsteeg, C.J., Dusoswa, S.A., Ting, D.T., Hickman, S., et al. (2019). Glioblastoma-Associated Microglia Reprogramming Is Mediated by Functional Transfer of Extracellular miR-21. Cell Rep *28*, 3105–3119.

Aftab, Q., Sin, W.C., and Naus, C.C. (2015). Reduction in gap junction intercellular communication promotes glioma migration. Oncotarget *6*, 11447–11464.

Al-Nedawi, K., Meehan, B., Micallef, J., Lhotak, V., May, L., Guha, A., and Rak, J. (2008). Intercellular transfer of the oncogenic receptor EGFRvIII by microvesicles derived from tumour cells. Nat. Cell Biol. *10*, 619–624.

Alcantara Llaguno, S., Chen, J., Kwon, C.H., Jackson, E.L., Li, Y., Burns, D.K., Alvarez-Buylla, A., and Parada, L.F. (2009). Malignant astrocytomas originate from neural stem/progenitor cells in a somatic tumor suppressor mouse model. Cancer Cell *15*, 45–56.

Assanah, M., Lochhead, R., Ogden, A., Bruce, J., Goldman, J., and Canoll, P. (2006). Glial progenitors in adult white matter are driven to form malignant gliomas by platelet-derived growth factor-expressing retroviruses. J. Neurosci. *26*, 6781–6790.

Bachoo, R.M., Maher, E.A., Ligon, K.L., Sharpless, N.E., Chan, S.S., You, M.J., Tang, Y., DeFrances, J., Stover, E., Weissleder, R., et al. (2002). Epidermal growth factor receptor and Ink4a/Arf: convergent mechanisms governing terminal differentiation and transformation along the neural stem cell to astrocyte axis. Cancer Cell *1*, 269–277.

Bjerkvig, R., Tysnes, B.B., Aboody, K.S., Najbauer, J., and Terzis, A.J. (2005). Opinion: the origin of the cancer stem cell: current controversies and new insights. Nat. Rev. Cancer *5*, 899–904.

Brennan, C.W., Verhaak, R.G., McKenna, A., Campos, B., Noushmehr, H., Salama, S.R., Zheng, S., Chakravarty, D., Sanborn, J.Z., Berman, S.H., et al.; TCGA Research Network (2013). The somatic genomic landscape of glioblastoma. Cell *155*, 462–477.

Brewer, G.J., and Torricelli, J.R. (2007). Isolation and culture of adult neurons and neurospheres. Nat. Protoc. *2*, 1490–1498.

Calabrese, C., Poppleton, H., Kocak, M., Hogg, T.L., Fuller, C., Hamner, B., Oh, E.Y., Gaber, M.W., Finklestein, D., Allen, M., et al. (2007). A perivascular niche for brain tumor stem cells. Cancer Cell *11*, 69–82.

Casper, K.B., Jones, K., and McCarthy, K.D. (2007). Characterization of astrocyte-specific conditional knockouts. Genesis *45*, 292–299.

Charles, N.A., Holland, E.C., Gilbertson, R., Glass, R., and Kettenmann, H. (2012). The brain tumor microenvironment. Glia *60*, 502–514.

Coniglio, S.J., and Segall, J.E. (2013). Review: molecular mechanism of microglia stimulated glioblastoma invasion. Matrix Biol. *32*, 372–380.

El-Andaloussi, S., Lee, Y., Lakhal-Littleton, S., Li, J., Seow, Y., Gardiner, C., Alvarez-Erviti, L., Sargent, I.L., and Wood, M.J. (2012). Exosome-mediated delivery of siRNA *in vitro* and *in vivo*. Nat. Protoc. *7*, 2112–2126.

Escola, J.M., Kleijmeer, M.J., Stoorvogel, W., Griffith, J.M., Yoshie, O., and Geuze, H.J. (1998). Selective enrichment of tetraspan proteins on the internal vesicles of multivesicular endosomes and on exosomes secreted by human B-lymphocytes. J. Biol. Chem. *273*, 20121–20127.

Eskiocak, U., Ramesh, V., Gill, J.G., Zhao, Z., Yuan, S.W., Wang, M., Vandergriff, T., Shackleton, M., Quintana, E., Johnson, T.M., et al. (2016). Synergistic effects of ion transporter and MAP kinase pathway inhibitors in melanoma. Nat. Commun. *7*, 12336.

Fan, J., Milosevic, R., Li, J., Bai, J., and Zhang, Y. (2019). The impact of neuroimaging advancement on neurocognitive evaluation in pediatric brain tumor survivors: A review. Brain Science Advances *5*, 117–127.

Ge, W.P., Miyawaki, A., Gage, F.H., Jan, Y.N., and Jan, L.Y. (2012). Local generation of glia is a major astrocyte source in postnatal cortex. Nature *484*, 376–380.

Gibbings, D.J., Ciaudo, C., Erhardt, M., and Voinnet, O. (2009). Multivesicular bodies associate with components of miRNA effector complexes and modulate miRNA activity. Nat. Cell Biol. *11*, 1143–1149.

Gilbertson, R.J., and Rich, J.N. (2007). Making a tumour's bed: glioblastoma stem cells and the vascular niche. Nat. Rev. Cancer *7*, 733–736.

Godlewski, J., Krichevsky, A.M., Johnson, M.D., Chiocca, E.A., and Bronisz, A. (2015). Belonging to a network—microRNAs, extracellular vesicles, and the glioblastoma microenvironment. Neuro. Oncol. *17*, 652–662.

Gourlay, J., Morokoff, A.P., Luwor, R.B., Zhu, H.J., Kaye, A.H., and Stylli, S.S. (2017). The emergent role of exosomes in glioma. J. Clin. Neurosci. *35*, 13–23.

Graner, M.W., Alzate, O., Dechkovskaia, A.M., Keene, J.D., Sampson, J.H., Mitchell, D.A., and Bigner, D.D. (2009). Proteomic and immunologic analyses of brain tumor exosomes. FASEB J. *23*, 1541–1557.

Heldin, C.H. (2013). Targeting the PDGF signaling pathway in tumor treatment. Cell Commun. Signal. *11*, 97.

Hong, X., Sin, W.C., Harris, A.L., and Naus, C.C. (2015). Gap junctions modulate glioma invasion by direct transfer of microRNA. Oncotarget *6*, 15566–15577.

Hoshino, A., Costa-Silva, B., Shen, T.L., Rodrigues, G., Hashimoto, A., Tesic Mark, M., Molina, H., Kohsaka, S., Di Giannatale, A., Ceder, S., et al. (2015). Tumour exosome integrins determine organotropic metastasis. Nature *527*, 329–335.

Iadecola, C., and Nedergaard, M. (2007). Glial regulation of the cerebral microvasculature. Nat. Neurosci. *10*, 1369–1376.

Jain, R.K., di Tomaso, E., Duda, D.G., Loeffler, J.S., Sorensen, A.G., and Batchelor, T.T. (2007). Angiogenesis in brain tumours. Nat. Rev. Neurosci. *8*, 610–622.

Jia, J.M., Chowdary, P.D., Gao, X., Ci, B., Li, W., Mulgaonkar, A., Plautz, E.J., Hassan, G., Kumar, A., Stowe, A.M., et al. (2017). Control of cerebral ischemia with magnetic nanoparticles. Nat. Methods *14*, 160–166.

Lässer, C., Eldh, M., and Lötvall, J. (2012). Isolation and characterization of RNA-containing exosomes. J. Vis. Exp., e3037. https://doi.org/10.3791/3037.

Le, D.M., Besson, A., Fogg, D.K., Choi, K.S., Waisman, D.M., Goodyer, C.G., Rewcastle, B., and Yong, V.W. (2003). Exploitation of astrocytes by glioma cells to facilitate invasiveness: a mechanism involving matrix metalloproteinase-2 and the urokinase-type plasminogen activator-plasmin cascade. J. Neurosci. *23*, 4034–4043.

Li, W., and Graeber, M.B. (2012). The molecular profile of microglia under the influence of glioma. Neuro. Oncol. *14*, 958–978.

Li, R., Li, G., Deng, L., Liu, Q., Dai, J., Shen, J., and Zhang, J. (2010). IL-6 augments the invasiveness of U87MG human glioblastoma multiforme cells via up-regulation of MMP-2 and fascin-1. Oncol. Rep. *23*, 1553–1559.

Li, C.C., Eaton, S.A., Young, P.E., Lee, M., Shuttleworth, R., Humphreys, D.T., Grau, G.E., Combes, V., Bebawy, M., Gong, J., et al. (2013). Glioma microvesicles carry selectively packaged coding and non-coding RNAs which alter gene expression in recipient cells. RNA Biol. *10*, 1333–1344.

Lindberg, N., Kastemar, M., Olofsson, T., Smits, A., and Uhrbom, L. (2009). Oligodendrocyte progenitor cells can act as cell of origin for experimental glioma. Oncogene *28*, 2266–2275.

Liu, C., Sage, J.C., Miller, M.R., Verhaak, R.G., Hippenmeyer, S., Vogel, H., Foreman, O., Bronson, R.T., Nishiyama, A., Luo, L., and Zong, H. (2011). Mosaic analysis with double markers reveals tumor cell of origin in glioma. Cell *146*, 209–221.

Lo Cicero, A., Stahl, P.D., and Raposo, G. (2015). Extracellular vesicles shuffling intercellular messages: for good or for bad. Curr. Opin. Cell Biol. *35*, 69–77.

Louis, D.N., Perry, A., Reifenberger, G., von Deimling, A., Figarella-Branger, D., Cavenee, W.K., Ohgaki, H., Wiestler, O.D., Kleihues, P., and Ellison, D.W. (2016). The 2016 World Health Organization Classification of Tumors of the Central Nervous System: a summary. Acta Neuropathol. *131*, 803–820.

Men, Y., Yelick, J., Jin, S., Tian, Y., Chiang, M.S.R., Higashimori, H., Brown, E., Jarvis, R., and Yang, Y. (2019). Exosome reporter mice reveal the involvement

of exosomes in mediating neuron to astroglia communication in the CNS. Nat. Commun. *10*, 4136.

Mistry, M., Zhukova, N., Merico, D., Rakopoulos, P., Krishnatry, R., Shago, M., Stavropoulos, J., Alon, N., Pole, J.D., Ray, P.N., et al. (2015). BRAF mutation and CDKN2A deletion define a clinically distinct subgroup of childhood secondary high-grade glioma. J. Clin. Oncol. *33*, 1015–1022.

Molofsky, A.V., Krencik, R., Ullian, E.M., Tsai, H.H., Deneen, B., Richardson, W.D., Barres, B.A., and Rowitch, D.H. (2012). Astrocytes and disease: a neurodevelopmental perspective. Genes Dev. *26*, 891–907.

Nakano, I., Garnier, D., Minata, M., and Rak, J. (2015). Extracellular vesicles in the biology of brain tumour stem cells—Implications for inter-cellular communication, therapy and biomarker development. Semin. Cell Dev. Biol. *40*, 17–26.

Osswald, M., Jung, E., Sahm, F., Solecki, G., Venkataramani, V., Blaes, J., Weil, S., Horstmann, H., Wiestler, B., Syed, M., et al. (2015). Brain tumour cells interconnect to a functional and resistant network. Nature *528*, 93–98.

Patel, A.P., Tirosh, I., Trombetta, J.J., Shalek, A.K., Gillespie, S.M., Wakimoto, H., Cahill, D.P., Nahed, B.V., Curry, W.T., Martuza, R.L., et al. (2014). Single-cell RNA-seq highlights intratumoral heterogeneity in primary glioblastoma. Science *344*, 1396–1401.

Persson, A.I., Petritsch, C., Swartling, F.J., Itsara, M., Sim, F.J., Auvergne, R., Goldenberg, D.D., Vandenberg, S.R., Nguyen, K.N., Yakovenko, S., et al. (2010). Non-stem cell origin for oligodendroglioma. Cancer Cell *18*, 669–682.

Placone, A.L., Quiñones-Hinojosa, A., and Searson, P.C. (2016). The role of astrocytes in the progression of brain cancer: complicating the picture of the tumor microenvironment. Tumour Biol. *37*, 61–69.

Rajendran, L., Bali, J., Barr, M.M., Court, F.A., Krämer-Albers, E.M., Picou, F., Raposo, G., van der Vos, K.E., van Niel, G., Wang, J., and Breakefield, X.O. (2014). Emerging roles of extracellular vesicles in the nervous system. J. Neurosci. *34*, 15482–15489.

Rath, B.H., Fair, J.M., Jamal, M., Camphausen, K., and Tofilon, P.J. (2013). Astrocytes enhance the invasion potential of glioblastoma stem-like cells. PLoS One *8*, e54752.

Ridder, K., Keller, S., Dams, M., Rupp, A.K., Schlaudraff, J., Del Turco, D., Starmann, J., Macas, J., Karpova, D., Devraj, K., et al. (2014). Extracellular vesicle-mediated transfer of genetic information between the hematopoietic system and the brain in response to inflammation. PLoS Biol. *12*, e1001874.

Roth, P., Junker, M., Tritschler, I., Mittelbronn, M., Dombrowski, Y., Breit, S.N., Tabatabai, G., Wick, W., Weller, M., and Wischhusen, J. (2010). GDF-15 contributes to proliferation and immune escape of malignant gliomas. Clin. Cancer Res. *16*, 3851–3859.

Seike, T., Fujita, K., Yamakawa, Y., Kido, M.A., Takiguchi, S., Teramoto, N., Iguchi, H., and Noda, M. (2011). Interaction between lung cancer cells and astrocytes via specific inflammatory cytokines in the microenvironment of brain metastasis. Clin. Exp. Metastasis *28*, 13–25.

Singh, S.K., Hawkins, C., Clarke, I.D., Squire, J.A., Bayani, J., Hide, T., Henkelman, R.M., Cusimano, M.D., and Dirks, P.B. (2004). Identification of human brain tumour initiating cells. Nature *432*, 396–401.

Singh, D.K., Kollipara, R.K., Vemireddy, V., Yang, X.L., Sun, Y., Regmi, N., Klingler, S., Hatanpaa, K.J., Raisanen, J., Cho, S.K., et al. (2017). Oncogenes Activate an Autonomous Transcriptional Regulatory Circuit That Drives Glioblastoma. Cell Rep. *18*, 961–976.

Skog, J., Würdinger, T., van Rijn, S., Meijer, D.H., Gainche, L., Sena-Esteves, M., Curry, W.T., Jr., Carter, B.S., Krichevsky, A.M., and Breakefield, X.O. (2008). Glioblastoma microvesicles transport RNA and proteins that promote tumour growth and provide diagnostic biomarkers. Nat. Cell Biol. *10*, 1470–1476.

Tashiro, A., Zhao, C., and Gage, F.H. (2006). Retrovirus-mediated single-cell gene knockout technique in adult newborn neurons *in vivo*. Nat. Protoc. *1*, 3049–3055.

Valadi, H., Ekström, K., Bossios, A., Sjöstrand, M., Lee, J.J., and Lötvall, J.O. (2007). Exosome-mediated transfer of mRNAs and microRNAs is a novel mechanism of genetic exchange between cells. Nat. Cell Biol. *9*, 654–659.

Venkataramani, V., Tanev, D.I., Strahle, C., Studier-Fischer, A., Fankhauser, L., Kessler, T., Körber, C., Kardorff, M., Ratliff, M., Xie, R., et al. (2019). Glutamatergic synaptic input to glioma cells drives brain tumour progression. Nature *573*, 532–538.

Venkatesh, H.S., Johung, T.B., Caretti, V., Noll, A., Tang, Y., Nagaraja, S., Gibson, E.M., Mount, C.W., Polepalli, J., Mitra, S.S., et al. (2015). Neuronal Activity Promotes Glioma Growth through Neuroligin-3 Secretion. Cell *161*, 803–816.

Venkatesh, H.S., Tam, L.T., Woo, P.J., Lennon, J., Nagaraja, S., Gillespie, S.M., Ni, J., Duveau, D.Y., Morris, P.J., Zhao, J.J., et al. (2017). Targeting neuronal activity-regulated neuroligin-3 dependency in high-grade glioma. Nature *549*, 533–537.

Venkatesh, H.S., Morishita, W., Geraghty, A.C., Silverbush, D., Gillespie, S.M., Arzt, M., Tam, L.T., Espenel, C., Ponnuswami, A., Ni, L., et al. (2019). Electrical and synaptic integration of glioma into neural circuits. Nature *573*, 539–545.

Verhaak, R.G., Hoadley, K.A., Purdom, E., Wang, V., Qi, Y., Wilkerson, M.D., Miller, C.R., Ding, L., Golub, T., Mesirov, J.P., et al.; Cancer Genome Atlas Research Network (2010). Integrated genomic analysis identifies clinically relevant subtypes of glioblastoma characterized by abnormalities in PDGFRA, IDH1, EGFR, and NF1. Cancer Cell *17*, 98–110.

Visvader, J.E. (2011). Cells of origin in cancer. Nature *469*, 314–322.

Wang, Y., Yang, J., Zheng, H., Tomasek, G.J., Zhang, P., McKeever, P.E., Lee, E.Y., and Zhu, Y. (2009). Expression of mutant p53 proteins implicates a lineage relationship between neural stem cells and malignant astrocytic glioma in a murine model. Cancer Cell *15*, 514–526.

Yang, Y., Ge, W., Chen, Y., Zhang, Z., Shen, W., Wu, C., Poo, M., and Duan, S. (2003). Contribution of astrocytes to hippocampal long-term potentiation through release of D-serine. Proc. Natl. Acad. Sci. USA *100*, 15194–15199.

Zeng, Q., Michael, I.P., Zhang, P., Saghafinia, S., Knott, G., Jiao, W., McCabe, B.D., Galván, J.A., Robinson, H.P.C., Zlobec, I., et al. (2019). Synaptic proximity enables NMDAR signalling to promote brain metastasis. Nature *573*, 526–531.

Zhang, W., Couldwell, W.T., Simard, M.F., Song, H., Lin, J.H., and Nedergaard, M. (1999). Direct gap junction communication between malignant glioma cells and astrocytes. Cancer Res. *59*, 1994–2003.

Zhang, L., Zhang, S., Yao, J., Lowery, F.J., Zhang, Q., Huang, W.C., Li, P., Li, M., Wang, X., Zhang, C., et al. (2015). Microenvironment-induced PTEN loss by exosomal microRNA primes brain metastasis outgrowth. Nature *527*, 100–104.

Zhu, Z., Kalyan, B.S., and Chen, L. (2019). Therapeutic potential role of exosomes for ischemic stroke. Brain Science Advances *5*, 128–143.

Zhu, Y., Harada, T., Liu, L., Lush, M.E., Guignard, F., Harada, C., Burns, D.K., Bajenaru, M.L., Gutmann, D.H., and Parada, L.F. (2005). Inactivation of NF1 in CNS causes increased glial progenitor proliferation and optic glioma formation. Development *132*, 5577–5588.

Zomer, A., Maynard, C., Verweij, F.J., Kamermans, A., Schäfer, R., Beerling, E., Schiffelers, R.M., de Wit, E., Berenguer, J., Ellenbroek, S.I.J., et al. (2015). *In Vivo* imaging reveals extracellular vesicle-mediated phenocopying of metastatic behavior. Cell *161*, 1046–1057.

# STAR★METHODS

## KEY RESOURCES TABLE

| REAGENT or RESOURCE | SOURCE | IDENTIFIER |
|---|---|---|
| Antibodies | | |
| Rat anti-CD31 | BD PharMingen | BD550274; RRID: AB_393571 |
| Rabbit anti-GFAP | Sigma-Aldrich | G9269; RRID: AB_477035 |
| Rabbit anti-Iba-1 | Wako Pure Chemical Industries | 019-19741; RRID: AB_839504 |
| Mouse anti-NeuN | Millipore | MAB377; RRID: AB_2298772 |
| Rat anti-PDGFRβ | eBioscience | 14-1402-81; RRID: AB_467492 |
| Rabbit anti-NG2 | Millipore | AB5320; RRID: AB_91789 |
| Rabbit anti-GluT1 | Thermofisher scientific | RB-9052-P0; RRID: AB_177894 |
| Bacterial and Virus Strains | | |
| shRab27a Mission shRNA Transduction Particles | Sigma-Aldrich | SHCLNV-NM_023635 |
| Chemicals, Peptides, and Recombinant Proteins | | |
| Exosome-Depleted FBS | Thermofisher scientific | A25904DG |
| Hoechst 33342 | Thermofisher scientific | H1399 |
| DAPI | Thermofisher scientific | D3571 |
| Experimental Models: Cell Lines | | |
| PS5A glioma | Robert Bachoo laboratory, (Singh et al., 2017) | n.a. |
| 73C glioma | Robert Bachoo laboratory, (Singh et al., 2017) | n.a. |
| OPC-HZ | Hui Zong laboratory (Liu et al., 2011) | n.a. |
| Experimental Models: Organisms/Strains | | |
| *Foxn1$^{-/-}$: B6.Cg-Foxn1 < nu > /JFoxn1$^{-/-}$,* | Jackson laboratory | No. 000819; RRID: IMSR_JAX:000819 |
| *Ai14: B6;129S6-Gt(ROSA)26Sortm14(CAG-tdTomato) Hze/J* | Jackson laboratory | No. 007908; RRID: IMSR_JAX:007908 |
| hGFAP-CreER: B6(C3)-Tg(GFAP-cre/Esr1)13Kdmc, | MMRRC | No.016992; RRID: MMRRC_016992-MU |
| Recombinant DNA | | |
| *CAG-GFP/cre* | Addgene, Tashiro et al., 2006 | 49054; RRID: Addgene_49054 |
| Software and Algorithms | | |
| Prism7 | GraphPad | https://www.graphpad.com/scientific-software/prism/ |
| ImageJ | NIH | https://imagej.nih.gov/ij/ |

## LEAD CONTACT AND MATERIALS AVAILABILITY

Further information and requests for resources and reagents should be directed to and will be fulfilled by the Lead Contact, Woo-Ping Ge (Woo-ping.Ge@UTSouthwestern.edu or Woopingge@cibr.ac.cn).

Glioma cell lines or plasmids generated in this study will be made available on request but we may require a completed Materials Transfer Agreement.

## EXPERIMENTAL MODEL AND SUBJECT DETAILS

Experimental procedures followed the guidelines of Institutional Animal Care and Use Committee at University of Texas Southwestern (UTSW) Medical Center. All efforts were made to minimize suffering and reduce the number of animals. Experiments were performed on adult C57BL/6 wild-type mice or immunodeficient nude mice *Foxn1$^{nu}$* (*Foxn1$^{-/-}$*) mice (Jackson laboratory) or *hGFAP-CreER* mice expressing Cre recombinase under the control of the hGFAP promoter crossed with Ai14 mice, which have a loxP-flanked STOP cassette preventing transcription of a CAG promoter-driven red fluorescent protein variant (tdTomato) - all inserted into the Gt(ROSA)26Sor locus (Jackson laboratory). We use mice of both sexes in this study.

## METHOD DETAILS

### Animals

All animal experiments were carried out in accordance with protocols approved by the Institutional Animal Care and Use Committee at University of Texas Southwestern (UTSW) Medical Center. The immunodeficient nude mice *Foxn1*$^{nu}$ (*Foxn1*$^{-/-}$, Stock No. 000819) and Cre recombinase dependent reporter mice *Ai14* (*ROSA26*$^{CAG\text{-}loxP\text{-}STOP\text{-}loxP\text{-}tdTomato}$) were purchased from the Jackson Laboratory. *Foxn1*$^{+/-}$*; Ai14* mice were produced by crossing nude and *Ai14* mice, and *Foxn*$^{-/-}$*; Ai14* were produced through backcrossing of *Foxn1*$^{+/-}$*; Ai14* with *Foxn1*$^{-/-}$ (we only used males) or *Foxn1*$^{+/-}$ mice (also see Figure S1), All *Foxn1*$^{-/-}$*; Ai14* mice that we used exhibited behavior normal for *Foxn1*$^{nu}$ mice. C57BL/6J mice were purchased from UTSW animal resource center. All mice were housed in ventilated cages under standard conditions.

### Glioma cell lines

73C glioma cells were obtained from Robert Bachoo's laboratory. They generated primary astrocyte cultures from neonatal mice that carried conditional mutations for *Pten*$^{f/f}$, *p53*$^{f/f}$, and *LSLBraf*$^{V600E}$. To delete tumor suppressor genes and activate the oncogene, astrocytes of early passage cultures were infected with adenoviruses containing Cre Recombinase (Singh et al., 2017). They chose these mutations because of the high prevalence of p53 pathway inactivation and loss of PTEN, while *BRAF*$^{V600E}$, a rare mutation in adult glioblastomas that is common in pediatric brain tumors, represents powerful co-activation of PI3K/AKT and MAPK/ERK signal transduction pathways. Both of these pathways are ubiquitously activated in malignant gliomas (Brennan et al., 2013). Transplantation of *p53*$^{-/-}$, *Pten*$^{-/-}$, and *Braf*$^{V600E}$ astrocytes produced intracranial tumors consistent with high-grade histopathology. OPC-HZ glioma cell line was obtained from Hui Zong laboratory. The cell line was established from tumor cells derived from the brain of the *NG2-Cre:Nf1*$^{fl/fl}$*:p53*$^{fl/fl}$*:MADM* mouse. PS5A is a highly invasion, extremely angiogenic tumor phenotype (Singh et al., 2017). This primary mouse glioma cell line was derived from the adult SVZ (NSC) from a germ-line *Ink4a/Arf*$^{-/-}$ mouse that had been crossed to a *Pten*$^{f/f}$ mouse. The primary neurosphere cultures were then treated with Adeno-Cre virus to generate *Ink4a*$^{-/-}$ *Pten*$^{-/-}$ neurospheres and these were then infected with a retro-EGFRvIII (puro-selected). This particular neurosphere derived glioma cell line, is therefore, *Ink4a/Arf*$^{-/-}$*Pten*$^{-/-}$*EGFRvIII*.

### Glioma cell culture

Mouse astrocyte-derived glioma cell line 73C and neural stem cell-derived glioma cell line PS5A were originally provided by Robert Bachoo's laboratory. 73C glioma cells were cultured in DMEM containing 10% fetal bovine serum (FBS) (Sigma-Aldrich). PS5A cells were cultured as free-floating neurospheres in medium consisting of Dulbecco's modified Eagle's medium plus F-12 (DMEM/F12, Life technologies), 1 mM L-glutamine, B-27 (Life Technologies), 20 ng/ml of EGF, and 20 ng/ml of FGF2 (Singh et al., 2017), 20ng/ml progesterone (Sigma) and 1% insulin transferrin selenium X (GIBCO). Mouse OPC-derived glioma cell line OPC-HZ was developed in Hui Zong's laboratory. OPC-HZ cells were cultured in neurobasal medium supplemented with Glutamax and B27 (Invitrogen).

### Purification of retroviruses and *in vitro* infection of glioma cells

Retroviral infection of glioma cells *in vitro* was performed according to a previously described protocol (Tashiro et al., 2006). Briefly, three plasmids (*pCAG-NLS-GFP-Cre-PRE* or *pCAG-NLS-GFP-PRE*, *pCMV-gp* and *CMV-vsvg*) were transfected into HEK 293T cells with PolyJet$^{TM}$ reagent (SignaGen Laboratories) or Lipofectamine 2000 (Invitrogen). Virus-containing supernatants were harvested 2 d after transfection by centrifuging twice at 65,000 g for 2 h (Optima$^{TM}$ Max-XP, Beckman). The virus pellet was resuspended in PBS and stored in $-80°C$ for following infection. We infected glioma cells by adding retroviruses (RVs) to the glioma cell culture medium with polybrene (optional, 10 μg/ml working concentration, Sigma) to increase the efficiency of infection. Cell culture medium was replaced with fresh medium 24h after RV infection.

### Cell sorting by flow cytometery

Glioma cells were trypsinized with 0.25% trypsin (Sigma-Aldrich) 72h after infection. GFP- or GFP/cre-expressing glioma cells were sorted out using a FACSAria (Becton Dickinson) (Eskiocak et al., 2016). Briefly, control glioma cells without GFP expression (i.e., without RV infection) were loaded onto the FACS to set the gate of background signal. GFP/cre- or GFP-expressing cells were sorted based on their GFP signals. The sorting gate was set to collect the 10% of the cell population with the most GFP fluorescence. The sorted cells were seeded in growth medium on a 24-well plate for amplification.

### Purification of EVs

EVs were purified from cell culture supernatant as described previously (El-Andaloussi et al., 2012). Briefly, EV depletion FBS (Thermo Fisher Scientific) was used in 73C-GFP/cre cell culturing. After collecting 30 mL cell culture medium, we subjected it to centrifugation (10 min, 300 g, 4°C) and removed the cell pellet. The supernatant was filtered through a 0.22 μm filter. Ultracentrifugation was then performed in polyallomer centrifuge tubes (Optiseal, Beckman 361625) at 120,000 g for 70 min at 4°C with a fixed-angle rotor

(Optima$^{TM}$ Max-XP, Beckman). The supernatant was carefully removed by decanting and pipetting. The EV pellet was resuspended in a small volume of HBSS (30–50 μl, without $Ca^{2+}$, $Mg^{2+}$) by pipetting multiple times. The EV suspension was used fresh for experiments on the same day.

### Glioma cell transplantation and EV injection

All glioma cells used for transplantation were passaged one day before transplantation, to reach 70–80% confluence after incubation overnight in a cell culture incubator. Cells were trypsinized and resuspended in Hank's Balanced Salt Solution (without $Ca^{2+}$, $Mg^{2+}$ HBSS). Cells were counted and a suspension was prepared with a density of $10^4$/μl. 1 μL cell suspension in HBSS was transplanted into the right hemisphere of mouse brains via a glass micropipette (Wiretrol, Drummond) with a 50 μm tip generated by a Micropipette Puller (P-97, Sutter Instrument Co.). Injection location was determined by a stereotaxic instrument (RWD life science Inc). Cells were constantly injected into the striatum (−2mm, 0.5mm, −2.5mm), thalamus (−1.5mm, −2mm, −3.5 mm), hippocampus (−3mm, −1.5mm, −2.2mm), or cerebral cortex (−3mm, −1.5mm, −1.6mm). Mice were then housed in an animal room for 2 weeks to 3 months to allow for glioma growth. For EVs, we injected 1 μL of EV suspension (in PBS) into a brain region as we did for glioma cells.

### Blood cell labeling

DiD lipophilic carbocyanine and aminostyryl tracer (Life Technologies) was used to label blood cells as we previously reported (Jia et al., 2017). Briefly, one or two drops (~20−30 μl) of blood were collected from the retro-orbital sinus in a sterilized Eppendorf tube containing 500 μL of HBSS with 10 mM EDTA to avoid blood coagulation. The blood was centrifuged at 150 × g for 5 min at RT to spin down blood cells. The pellet was resuspended in 1 mL of HBSS with 7 μM (~7 μl) of DiD solution and gently mixed well. The mixture was incubated in 37 °C for 15 min, mixed gently every 5 min. Labeled blood cells were washed twice with HBSS and then centrifuged and resuspended in 200 μL HBSS. About 50–100 μL of solution with DiD-labeled cells was injected back into the same mouse through its tail vein. DiD dye was excited with a 633nm laser (Zeiss LSM710).

### Mouse thinned-skull and opened-skull preparations

We anesthetized mice with a ketamine (60 mg $kg^{-1}$ i.p.) and xylazine (10 mg $kg^{-1}$ i.p.) cocktail. We made a craniotomy (3 mm in diameter) over the cerebral cortex, centered 2–3mm posterior to the bregma and 2–3 mm from the midline. Mice were fixed in a stereotaxic frame, a homemade mini-heating pad was utilized to keep the body temperature up, and eye ointment (Rugby) was applied to prevent the eyes from drying out. Carprofen (5 mg/Kg) and buprenorphine HCl (0.05–0.1mg/Kg) (UTSW Animal Research Center) were injected subcutaneously to prevent brain inflammation and ameliorate pain, respectively. For thinned-skull preparation, a microdrill (Foredom) with burrs (Fine Science Tools) was utilized to thin the skull bone to the inner cortical bone ~20 μm in thickness after removal of the skin over the top of the skull. The thinned skull was coated with a layer of cyanoacrylate glue (KaVo Kerr, optibond) and covered with a glass coverslip over the skull window. For opened-skull preparation, the periosteum was retracted to the edges of the skull using a scalpel. Cyanocrylate-based glue was applied in a thin layer over the entire exposed skull to reduce mobility of the skull bone joints. After drawing a circle (2–3mm in diameter) with a marker pen on the region where the cranial window was created, we drilled along the circle with a microdrill. The piece of skull was lifted and removed, and cold saline-soaked absorbable gelatin sponge (Gelfoam) was used to prevent bleeding of the dura. A sterile donut-shaped glass coverslip (2 mm in diameter) was installed on top of the dura mater. A very small drop of cyanocrylate-based glue was applied around the window. We secured the coverslip by applying dental adhesive cement (Prime Dent) around it and covered the entire exposed skull with the glue in a thick layer to attach a titanium plate with a hole on top of the coverslip. This plate was later used to attach the mice securely onto the stage of our microscope for live imaging. We covered the glass window with a piece of black tape to prevent dust and light from entering. The stage level was carefully adjusted to ensure the cranial window was parallel to the microscope lens glass when imaging.

### Longitudinal time-lapse imaging *in vivo*

Mice with glioma cell transplantation were imaged on an upright two-photon excitation microscope (Zeiss LSM710 NLO). Blood flow was visualized by DiD-labeled blood cells (see details above). We used a 20 × (N.A. 1.0) water-immersion objective lens for imaging. Glioma cells, non-glioma brain cells, and blood cells were scanned with XYZ mode for time-lapse imaging as we previously reported (Ge et al., 2012; Jia et al., 2017). The same imaging area was located repeatedly according to the branching pattern of major blood vessels, and Z stack images were scanned every 1–2 d in the following 1–3 weeks after day 6 post-injection. During imaging, mice were anaesthetized with 1−2% isoflurane in oxygen, and their body temperature was kept up with a home-made heating pad (10 × 5 cm). GFP was excited with a 488nm or 860nm Infrared (IR) laser, tdTomato with a 543 nm or 930−960 nm IR laser, and DiD was excited with a 633nm laser. Mice were housed in their home cages after imaging.

### Immunostaining

Mice were perfused transcardially with PBS followed by 4% (w/v) paraformaldehyde (PFA). The brain was fixed in cold PFA (4°C) for 2–3 h, washed thoroughly in PBS overnight, and dehydrated sequentially by 15% and 30% sucrose in PBS. Fixed brains were sectioned at 10–20 μm with a cryostat (model CM3050S, Leica) or 50–70 μm with a vibrotome (VT1000S, Leica). Sections were stained as we described previously (Ge et al., 2012). Briefly, sections were permeabilized with 0.25% Triton X-100 and then blocked with 5% BSA and 3% normal goat serum with 0.25% Triton X-100 for 2 h. Primary antibodies against GFAP (1:300 rabbit, Sigma,

G9269), Iba1 (1:300, rabbit, Wako Pure Chemical Industries, 019-19741), NeuN (1:300, mouse, MAB377, Millipore), PDGFRβ (1:300, Rat, eBioscience, 14-1402-81), or NG2 (1:300, AB5320, rabbit, polyclonal, Millipore), GluT1 (1:300, Rabbit, Thermofisher, RB-9052-P0), CD31 (1:50, Rat, BD550274), and GABA (1:300, Rabbit, Sigma-Aldrich A2052) were incubated with brain sections for 24−48 h at 4°C. After three washes in PBS together with Hoechst33342 or DAPI (Life Technologies), sections were incubated with secondary antibodies conjugated with Alexa 488, Alexa 546, or Alexa 633/647 (1:500, Life Technologies) for 2 h at RT (22−25°C). After three washes in PBS, sections were mounted with anti-fade mounting medium Fluoro-Gel (EMS). Whole-brain section images were taken with the tilling scan function on inverted confocal microscope (Zeiss LSM780) with 8% overlapping of adjacent tiles for automatic stitching.

### Reverse transcription polymerase chain reaction (RT-PCR)

Total RNA of cells and EVs was isolated using RNeasy Plus Mini Kit (QIAGEN) following the manufacturer's protocol. cDNA library was prepared using iScript Reverse Transcription Supermix for RT-qPCR (Bio-Rad) following the manufacturer's protocol. PCR primers for EGFP (F: 5′-AAGTTCATCTGCACCACCG-3′, R: 5′-TCCTTGAAGAAGATGGTGCG), Cre (F: 5′-GGTCGATGCAACGAGT GATGA-3′, R: 5′-GCTAAGTGCCTTCTCTACACC-3′), and mouse GAPDH (F: 5′-ACCCAGAAGACTGTGGATGG-3′, R: 5′-CACATT GGGGTAGGAACAC-3′) were synthesized by IDT (Integrated DNA Technologies), and DNA fragments were amplified using a normal PCR protocol with 2 × Taq PCR Premix reagent (Bioland scientific).

### Whole-cell recording of glioma cells

Whole-cell recordings from cultured glioma cells were done with an upright microscope (Olympus, BX51WI). Recording pipettes were filled following a routine protocol with a solution containing 125 mM potassium gluconate, 15 mM KCl, 10 mM HEPES, 3 mM MgATP, 0.3 mM Na-GTP, 5 mM Na-phosphocreatine, and 0.2 mM EGTA (pH 7.2–7.4, 290–300 mosM). Membrane potential in voltage-clamp mode was held at −60 mV. Signals filtered with amplifier circuitry were sampled at 10 kHz and analyzed using Axon CLAMPEX 10.0 (Molecular Devices).

### Whole-cell recording of neurons in brain slices

Adult mouse brains (> P70) with PS5A or OPC-ZH glioma transplantation were acutely dissected out on DPI30. We prepared slices (400 μm in thickness) as described previously (Ge et al., 2012). Briefly, mouse brains were dissected and sectioned with a Leica vibratome (VT-1000S) in ice-cold oxygenated (5% $CO_2$ and 95% $O_2$) artificial cerebrospinal fluid solution (ACSF, in mM: 124 NaCl, 5 KCl, 2.6 $CaCl_2$, 1.3 $MgSO_4$, 1.25 $NaH_2PO_4$, 26 $NaHCO_3$ and 10 Glucose). Transverse slices were maintained in ACSF before recording. Both labeled neurons (i.e., receiving Cre from glioma cells) and unlabeled neighboring neurons were recorded with gap-free mode for 2 min under voltage-clamp mode for recording spontaneous postsynaptic response and current-clamp mode for recording action potential pattern. Neuronal membrane potential in voltage-clamp mode was held at −60 mV. Data were analyzed with Clampfit10.0 and miniAnalysis.

### Microfluidic channel imaging

Both mouse (73 C, PS5A) and patient human glioma cells (R548) were used. To fabricate the poly dimethylsiloxane (PDMS) based microfluidic channels (10 × 20 × 530 μm) used, silicon molds were first prepared using standard photolithography. Briefly, positive molds of the microfluidic channels were fashioned first using SU-8 5 (Microchem Corp, Newton, MA) deposited to 10μm height on silicon wafer followed by positive molds of reservoirs at each end of the microfluidic channels using SU-8 50 (Microchem Corp, Newton, MA) deposited to a 100 μm height by the double deposition method. Each layer was deposited, aligned, photo-patterned, developed using SU-8 developer and rinsed using isopropanol. PDMS (Sylgard 184 Silicone Elastomer Base, Dow Corning) mixed with the curing agent (Sylgard 184 Silicone Elastomer Curing Agent, Dow Corning) at 10:1 (v/v) ratio was then poured onto the mold to a height of ~5.0 mm and cured at 150°C for 10min. After curing, the PDMS device formed was peeled off and punched at the reservoir positions to create an inlet and an outlet. The device was then washed with 70% ethanol, air plasma treated using a UV-Ozone cleaner (PSD Pro Series, Novascan) and assembled onto a sterilized glass coverslip. Prior to plating with cells, the assembled PDMS devices were treated using 10ug/ml laminin. The cells were plated at a density of 2.5 × $10^5$ cells in the inlet reservoir and their migration properties through confined channels assessed by time lapse microscope using differential interference contrast Microscopy (Zeiss AxioVert 200M Inverted Microscope, 40 × /NA0.95) every 10 s at typical culture conditions. To allow for spontaneous entry into the channels, no chemotactic gradient was introduced.

### Cell fusion analysis with flow cytometery

*Ai14* tg mouse brains transplanted with 73C-GFP/cre glioma cells were dissected out at DPI13. Individual tdTomato$^+$ cells in and around tumors were isolated as described previously (Brewer and Torricelli, 2007). Fixed isolated brain cells (with PFA) of each mouse were subjected to flow cytometry analysis on FACS LSRFortessa SORP system (BD). Laser wavelengths of 405 nm, 488 nm, and 561 nm were employed to detect GFP, tdTomato and DAPI (2N for normal cells or 4N for fused cells or dividing cells). Data obtained via flow cytometry were then processed on FlowJo software.

### Imaging EVs with Electron Microscopy

To verify the presence of EVs, the preparations were analyzed by using transmission electron microscopy (TEM; Tacnai). Briefly, 5 μL EVs were fixed in 2% PFA after purification of EVs (see above). EVs were allowed to attach to Formvar/Carbon-coated Film (FCF200) grids for 1 min, followed by negative staining using 2% Uranyl Acetate (UA) solution for 1 min. EVs were observed under EM at 80kV, and images were acquired using Morada digital camera and iTEM software (Olympus). The size of EVs was analyzed with ImageJ.

### Evaluation of 73C cell growth with or without knockdown of Rab27a

73C cells were infected by LV with *Rab27a* targeted shRNA or LV with scrambled control and selected by puromycin for 7d to remove non-infected cells. Cells were then seeded in a 6-well plate at the same density on d0, and images were acquired randomly from 5 regions of each well on d0, d1, d2 and d3. The cell densities from all images were analyzed with ImageJ.

### Transwell test of EV uptake by primary cultured astrocytes

Primary astrocytes were isolated from the cerebral cortex of P0 wild-type C57BL/6J mouse pups as previously described (Yang et al., 2003) and cultured on poly-D-lysine-coated glass coverslips in a 6-well plate. Transwells (Corning) with 0.4 μm pore membrane were sitting on top of the astrocyte layer. 73C cells with CD63-GFP overexpression were seeded on the membrane in transwells. Astrocytes and 73C glioma cells were co-cultured in the same media (DMEM with 10% FBS) for 48h. Astrocytes attached to coverslips were gently washed with HBSS for 3 times and were then fixed in 4% PFA for 20 min. Astrocytes were stained with Hoechst33342 for nucleus labeling before imaging under a confocal microscope.

## QUANTIFICATION AND STATISTICAL ANALYSIS

All of the statistical details of experiments can be found in the figure legends and methods, including the statistical tests used, exact value of n, what n represents (e.g., number of animals, number of cells, etc.) and precision measures (e.g., mean, SEM).

## DATA AND CODE AVAILABILITY

This study did not generate/analyze datasets or code.